Algorithms for numerical simulation of radio-frequency glow discharges

Ajit P. Paranjpe
Department of Mechanical Engineering, Stanford University, Stanford, California 94305

James P. McVittie
Integrated Circuits Laboratory, Stanford University, Stanford, California 94305

Sidney A. Self
Department of Mechanical Engineering, Stanford University, Stanford, California 94305
(Received 28 September 1989)

A fast and numerically stable technique has been developed for the numerical simulation of parallel-plate rf glow discharges, operating at frequencies exceeding ~10 MHz. In such discharges the ion concentrations do not vary on the time scale of the rf cycle. Thus the transport equations for charged particles can be decoupled into a set of time-averaged and time-dependent equations. Rather than follow the evolution of the discharge following initiation, a solution of the time-averaged equations provides the steady-state solution directly. Once the time-averaged solution is known, a solution of the time-dependent equations yields the modulation of the time-dependent variables about their time-averaged value. Decoupling of the equations also reduces the number of variables at each step, thereby enabling optimization of matrix solutions for the system of nonlinear equations. Finally, good initial guesses are provided by solutions of simplified models. Electron kinetics and transport data are obtained by solving the zero-dimensional Boltzmann equation for electrons in conjunction with a model for the kinetics of excited states. Simulations have been performed for discharges in Ar and SF_6. A typical case for an argon discharge is executed in 6 min on a Micro Vax II Computer as compared to twice as many minutes on a Cray computer for similar models reported by other workers. Results of the simulations are in agreement with those reported elsewhere and with measurements made using a tuned Langmuir probe.

I. INTRODUCTION

The widespread use of parallel-plate rf discharges for dry processing has stimulated numerous papers on numerical simulation of these discharges. While many of the models developed do not treat the entire problem in a self-consistent fashion, recent efforts have partially rectified this shortcoming.[1-6] Continuum models are based on a self-consistent solution of the transport equations for charged particles coupled with Poisson's equation, for specified discharge conditions. A self-consistent solution of the discharge is essential in order to qualitatively reproduce many of the experimentally observed features of time- and space-resolved electron-impact excitation.[7] Long solution times and a tendency towards numerical instability make traditional solution techniques for the fluid equations unsuitable for use in a robust rf discharge simulator.

This paper describes a fast and numerically stable technique for solving the fluid equations for a high-frequency (> 10 MHz) rf parallel-plate glow discharge in a variety of gases. The technique was first developed for electropositive gases,[8] and has since been extended to electronegative gases. In particular, discharges in Ar and SF_6 have been considered. Typical solution times are of the order of 6 min on a MicroVax II computer for discharges in electropositive gases, and twice as long for discharges in electronegative gases. This represents significant savings in computer time compared to several minutes on a Cray computer for similar models reported by other workers.[5] The algorithm is between two and three orders of magnitude faster than existing schemes. Three advances have made this possible.

(i) Limiting the domain of applicability to frequencies above the ion plasma frequency (> 10 MHz) permits the systematic decoupling of the equations into a set of time-averaged and time-dependent equations. By recognizing that in high-frequency rf discharges, many of the variables do not vary on the time scale of the rf cycle, the set of equations can be simplified through time averaging. By solving the set of time-averaged equations, the periodic steady-state solution can be obtained directly, rather than having to follow the evolution of the discharge. Once the time-averaged solution is known, the time-dependent equations for those variables that are modulated on the time scale of the rf cycle are solved in order to determine the extent of the modulation about their time-averaged values. Thus the principal saving in computer time arises from proceeding directly to the steady-state solution rather than following the evolution of the discharge, which occurs over thousands of rf cycles. With the approach described here, periodic steady state is achieved within ten rf cycles, compared to 10 000 using the conventional approach.[5,9] The other disadvantage of following the evolution of the discharge is that eventually changes in discharge parameters from cycle to cycle are so small that one might assume that harmonic steady state has been achieved. Even after prolonged execution,

numerical error may prevent periodic steady state from being achieved. This may be the cause of the nonphysical dip in the electron concentration at center of the discharge, in the simulations presented in Ref. 10.

(ii) The decoupling reduces the number of variables at each step, and matrix solutions of the nonlinear equations can be optimized. If the equations are not decoupled, one has to solve for eight variables simultaneously; one for each of the eight equations. In the algorithms developed here, at most two parameters are treated as variables simultaneously.

(iii) The number of rf cycles required for convergence is significantly reduced if a good initial guess for the solution is available. Solutions of simplified models can provide these estimates. Simplified models have been formulated for discharges in electropositive and electronegative gases. These models capture the essential physics, and provide reasonable accuracy in estimating certain discharge parameters. If such accuracy is acceptable, a solution of the comprehensive model is avoided. Simulations performed for the simplified models are an order of magnitude faster than the full simulation.

II. MODEL DESCRIPTION

In many gases a continuum description is appropriate at pressures exceeding ~ 300 mTorr. The continuum model consists of equations, which for a one-dimensional (1D) Cartesian coordinate system are

$$\frac{\partial n_e}{\partial t}+\frac{\partial \Gamma_e}{\partial x}=r_i-r_a+r_d \ , \tag{1}$$

$$\frac{\partial n_p}{\partial t}+\frac{\partial \Gamma_p}{\partial x}=r_i-k_r n_n n_p \ , \tag{2}$$

$$\frac{\partial n_n}{\partial t}+\frac{\partial \Gamma_n}{\partial x}=r_a-k_r n_n n_p-r_d \ , \tag{3}$$

$$\Gamma_e \equiv -n_e v_e=-\mu_e n_e E-D_e\frac{\partial n_e}{\partial x} \ , \tag{4}$$

$$\Gamma_p \equiv n_p v_p=\mu_p n_p E-\frac{n_p}{\nu_h}\frac{\partial v_p}{\partial t} \ , \tag{5}$$

$$\Gamma_n \equiv n_n v_n=-\mu_n n_n E-\frac{n_n}{\nu_h}\frac{\partial v_n}{\partial t} \ , \tag{6}$$

$$\frac{\partial E}{\partial x}=\frac{e}{\epsilon_0}(n_p-n_n-n_e) \ , \tag{7}$$

$$\frac{\partial(n_e u_e)}{\partial t}+\frac{5}{3}\frac{\partial(\Gamma_e u_e)}{\partial x}-\frac{2}{3}\frac{\partial(K_e/k)}{\partial x}\frac{\partial u_e}{\partial x}+\Gamma_e E+k_\epsilon(u_e)n_e N=0 \ . \tag{8}$$

Here x (cm) is the distance from the grounded electrode, t (s) is the time coordinate, and the subscripts e, p, and n refer to electrons, positive ions, and negative ions, respectively. Charged-particle concentrations (cm^{-3}) are denoted by n, charged-particle fluxes ($cm^{-2}s^{-1}$) by Γ, charged-particle velocities (cm/s) by v, charged-particle mobilities ($cm^2/V\,s$) by μ, and the electron diffusion coefficient (cm^2/s) by D_e. Also u_e (eV) is the mean electron energy; E (V/cm) is the electric field; $K_e=3n_e kD_e/2$ is the electron thermal conductivity (W/cm K); r_i, r_a, and r_d are the ionization, attachment, and detachment rates ($cm^{-3}s^{-1}$); k_r is the rate constant (cm^3/s) for recombination; $k_\epsilon(u_e)$ is the electron-energy-loss rate ($eV\,cm^3/s$); $k\,(J/K)$ is the Boltzmann constant, $e(C)$ is the electronic charge, ϵ_0(F/cm) is the permittivity of free space; and N (cm^{-3}) is the gas number density.

This general formulation was first suggested by Graves and Jensen,[1] but for a symmetric discharge in an electropositive gas. Additional terms in the continuity equations arise from attachment[2] and detachment.[11] At pressures below ~ 300 mTorr and in regions of intense fields where the ion and electron velocity distributions are highly anisotropic, the fluid equations provide only a partial representation of the physics.

Equations (1)–(3), which are the continuity equations for charged particles, involve terms arising from ionization, attachment, detachment, ion-ion recombination, and ambipolar diffusion. The recombination of electrons and positive ions is negligible in low-pressure glow discharges. In SF_6 discharges negative ions are lost primarily through ion-ion recombination, while in O_2 discharges collisional detachment of negative ions dominates over ion-ion recombination. The time-averaged ionization and attachment rates r_i and r_a, which appear in the continuity equations, are calculated iteratively (explained later) according to

$$r_i=\frac{1}{T}\int_0^T k_i n_e N\,dt \ , \tag{9}$$

$$r_a=\frac{1}{T}\int_0^T k_a n_e N\,dt \ , \tag{10}$$

where k_i and k_a, the rate constants ($cm^{-3}s^{-1}$) for ionization and attachment, respectively, are functions of the mean electron energy, and are derived from the Townsend ionization and attachment coefficients. In O_2 discharges, the detachment rate may be expressed as $k_d n_n N^*$, where N^* is the concentration of excited O_2, and k_d is the rate constant for detachment. Using the time-averaged rates rather than the instantaneous rates in the continuity equations is adequate since fluctuations in electron concentration are due primarily to changes in the electric field and not due to modulation of the ionization and attachment rates. However, since the electron energy may be modulated quite significantly, it is essential to account for the time-dependence of the ionization and attachment rates, in order to evaluate the time-averaged quantities.

In Eq. (4), which is the momentum conservation equation for electrons, the inertia terms have been neglected. In the collision-dominated regime, electrons respond to the instantaneous field at rf frequencies, and inertia terms are unimportant. In contrast the ions, being massive, do not respond to the time-varying field, but rather to the time-averaged field. However, depending on the frequency, their velocity is modulated somewhat. Thus in Eqs. (5) and (6), the momentum conservation equations for ions, the local acceleration term $(n_p/\nu_h \partial v_p/\partial t, n_n/\nu_h \partial v_n/\partial t)$ is retained.[3] For the

domain of this model the convective acceleration term $[v_p(\partial v_p/\partial x), v_n(\partial v_n/\partial_x)]$ is negligible compared to ion drift and has been neglected. Also ion diffusion is negligible compared to ion drift, and the ion diffusion term can be ignored. Since the magnetic fields have negligible effect on electron and ion motion, of the set of Maxwell's equations, only Poisson's equation [Eq. (7)] is relevant.

In the electron-energy balance equation [Eq. (8)], the second term refers to enthalpy transport through electron convection, the third to heat conduction, the fourth to joule heating and/or cooling, and the fifth refers to the electronenergy loss through elastic and inelastic collisions.

Instead of using the complete electron energy balance equation, the *local field approximation* has been used by several workers.[2,4] In the *local field approximation* the electrons are assumed to be in equilibrium with the local field, and the electron swarm parameters are then a function of the instantaneous local reduced electric field (E/N). The *local field approximation* fails under two circumstances. In the sheath regions the elastic field is large, but the Townsend ionization coefficient is low since the electrons are diffusing against the field. Also, at sufficiently low pressures or for high excitation frequencies, the electron energy distribution function may not be modulated very strongly, and the electrons may not be in equilibrium with the field. In short, the concept is valid provided the length scale of variations in the electric field is much longer than the electron mean free path. The *local field approximation* is improved by using the concept of an effective electric field. The effective electric field is an equivalent dc field that sustains the same electron-energy distribution function as exists in the rf discharge.[6]

The electron-energy distribution function in glow discharges is significantly non-Maxwellian, and ideally, the traditional electron-energy balance equation should be replaced by the time and space-dependent Boltzmann equation. Rather than adopt this computationally expensive approach, one can use electron transport data and Townsend ionization coefficients generated from a zero-dimensional solution of the Boltzmann equation for electrons. These data are usually parametrized in terms of the mean electron energy[3] or expressed in terms of an Arrhenius-type expression.[1] Rather than base k_ϵ on the local field, it is based on the mean electron energy. This is because in the regions of maximum power deposition, both the mobility (drift) and diffusion terms (rather than the drift term alone) are important in the expression for the electron drift velocity. Since the drift and diffusion terms oppose each other, the actual electron velocity is less than that calculated by the Boltzmann code for the same E/N. The Boltzmann equation solver essentially performs a zero-dimensional electron energy balance for an implied power deposition density of ev_eE $(=e\mu_eE^2)$. Thus, for a given E/N, the effective power deposition density calculated using the Boltzmann equation is higher than the power deposition density in the sheath of an rf discharge. In other words, for a given E/N, electrons are likely to be more energetic in a drift tube compared to the sheath of an rf discharge. On the other hand, the electron-energy distribution functions in a drift tube, and in the sheath of an rf discharge are likely to be equivalent to first order, if the mean electron energies in the two are the same. This suggests that rate constants for electron impact processes based on the mean electron energy, rather than the local field, are likely to be more representative. Characterizing the electron-energy distribution function in terms of the mean electron energy is inaccurate in regions of sharp gradients in the electron number density and the electric field. In such regions, the electron velocity distribution is quite anisotropic. This difficulty might be circumvented by specifying additional properties of the distribution function, or by solving the spatially dependent Boltzmann equation. Both options are infeasible at the present time. Another limitation of the electron-energy balance equation arises from the difference in characteristic times for energy relaxation between different parts of the distribution function. Frequently the tail of the distribution relaxes faster than its low-energy portion.[12] The higher the mean electron energy, the shorter is the energy relaxation time. Consequently, when the mean electron energy is high, the ionization rate is more nearly in equilibrium with the local field. Excited atomic and molecular states can have a profound impact on the electron swarm parameters. By coupling the zero-dimensional solution with a model for the kinetics of excited states, more realistic swarm data can be derived.[6,8]

The mode of energy coupling to the electrons by the electric field depends on the discharge operating conditions. In electronegative gases, the electric field is relatively large even in the plasma, and consequently ionization in the plasma sustains the discharge. In electropositive gases, at pressures which result in collisional sheaths, and at low-power levels, most of the ionization is due to plasma electrons and occurs at the plasma-sheath boundary. At higher-power levels, lower pressures, or lower frequencies, the secondary electrons emitted by energetic ion bombardment of the electrode are accelerated by the sheath potential drop forming a beamlike distribution (i.e., their random velocity is much smaller than their directed velocity), and contribute significantly to the total ionization. Even when ionization is dominated by plasma electrons, secondary electrons can have an effect on highly activated processes in the sheath. A single electron-energy balance equation can be written provided electrons formed through ionization in the plasma are indistinguishable from secondary electrons emitted from the electrodes. At low pressures or high-power levels the discharge may operate in the γ mode,[9] and ionization by secondary electrons sustains the discharge. Under these conditions, the secondary electrons are beamlike. Also, their mean energy far exceeds the energy of the plasma electrons and they contribute to most of the ionization. These two classes of electrons need to be treated as separate species, with an individual energy balance equation for each one.[9] The continuity equations for beam and plasma electrons are coupled since beam electrons upon dissipating energy via collisions become plasma electrons. The beam electron equations are an approximation to reality, but give qualitatively correct results under some circumstances. Even for plasma electrons,

the simple electron energy conservation equation is inappropriate when the electrons gain energy stochastically by interacting with the oscillating sheath. Under these conditions, only a small fraction of the energy gained from the field is converted into random energy that is describable with a mean energy. However, this phenomenon occurs at pressures below ~ 10 mTorr,[13] which is outside the realm of typical conditions. All these factors limit the applicability of Eq. (8).

The continuity equations yield the charged-particle concentrations, the momentum conservation equations yield the charged-particle fluxes, Poisson's equation yields the electric field, and the electron-energy balance equation yields the mean electron energy, and consequently the ionization and attachment rates. Boundary conditions are required for each of the equations. The boundary conditions have to be expressed at the grounded electrode ($x=0$) and at the powered electrode ($x=d$). The boundary conditions at the electrodes are

$$\Gamma_e = \mp S n_e - \gamma \Gamma_p \ , \tag{11}$$

$$\frac{\partial \Gamma_p}{\partial x} \approx 0 \Longrightarrow \frac{\partial^2 E^2}{\partial x^2} = 0 \ , \tag{12}$$

$$\Gamma_n = 0 \ , \tag{13}$$

$$\Gamma_c = \frac{J_{c0}}{e}\cos(\omega t) = \Gamma_p - \Gamma_n - \Gamma_e + \frac{\epsilon_0}{e}\frac{\partial E}{\partial t} \ , \tag{14}$$

$$q_e = \mp \tfrac{5}{3} u_e S n_e \ . \tag{15}$$

In the above expressions, S is an effective surface recombination velocity (cm/s), γ is the secondary electron emission coefficient, J_{c0} is the specified current density at the powered electrode, and q_e is the electron-energy flux to the electrode. When the continuity and momentum conservation equations are combined, a second-order partial-differential equation results. Equation (11) provides the two boundary conditions required for the electron continuity and momentum conservation equations. The surface recombination velocity, a concept borrowed from semiconductor device simulation,[7] is a phenomenological way of representing the electron recombination rate at the electrode. Clearly, a value $S=\bar{C}_e/4$ implies that the entire one-way flux of electrons towards the electrode is absorbed by the electrode. Lower values imply that some of the electrons are reflected. As long as $S > 10^5$ cm/s, the solution is insensitive to the exact value of S. In fact, since $n_e \ll n_p$ at the electrodes (except for a short duration during the anodic portion of the cycle), assuming that $n_e=0$ is also acceptable.[1] The second term on the right-hand side in Eq. (11) represents the secondary electron emission emission due to ion bombardment.

The boundary condition for positive ions [Eq. (12)] requires some explanation. Near the electrode, the rates for ionization and ion-ion recombination are virtually zero. Recognizing that at the electrode $n_n \ll n_e \ll n_p$ and expressing n_p in terms of the field using Eq. (7), the boundary condition $\partial^2 E^2/\partial x^2 = 0$ is obtained. Others have set either the positive-ion number density[3] or its gradient[1] to zero at the electrodes. A zero positive-ion number density implies an infinite electric field for a nonzero positive-ion flux ($\Gamma_p \approx \mu_p n_p E$). Setting the gradient to zero is equivalent to specifying that $E \sim x$ at the electrode. The present boundary condition is equivalent to specifying that $E \sim x^{1/2}$, which is in agreement with space-charge limited ion motion through a collision-dominated sheath. The choice of boundary conditions for the ion continuity equation is *ad hoc*. A proper treatment requires the inclusion of a thin ion diffusion boundary layer at the electrode surface.[1] All the boundary conditions are arbitrary to some extent, but since we are not interested in the details of the ion concentration very near the electrode, all the boundary conditions listed above lead to "satisfactory" results.

Negative ions cannot overcome the retarding potential of the sheath and are trapped in the plasma. As long as negative ions are not emitted by the electrode, the negative-ion flux at the electrode must be zero [Eq. (13)]. Since $\Gamma_n \approx -\mu_n n_n E$ and E is nonzero at the electrodes, an equivalent boundary condition is $n_n = 0$.

A variety of boundary conditions have been used for Poisson's equation. In this simulation, the total current density [$J_{c0}\cos(\omega t)$] is specified[5] at the powered electrode [Eq. (14)]. The total current is an algebraic sum of the electron, positive-ion, and negative-ion conduction currents, and the displacement current [$\epsilon_0(\partial E/\partial t)$]. Specifying the current provides a very powerful constraint since the current must be continuous through the discharge. Alternatively the discharge voltage at the powered electrode may be specified.[1] In practice, the discharge voltage and current are determined by the characteristics of the matching network and the rf supply. Strictly the current and voltage wave forms ought to be obtained self-consistently by considering the response of the matching network and the rf power supply driving the discharge. This has been done in the simulations by Barnes, Colter, and Elta.[4] The nature of the solution technique used here requires the current through the discharge to be specified. This is not a serious limitation since the current waveform in many discharges appears sinusoidal, while the voltage waveform is sometimes clipped at the extremities.

The boundary condition for the electron-energy balance equation developed by Chung[14] for the cases of absorbing and emitting surfaces is used. If one compares Eq. (15) with Eq. (8), the boundary condition for the electron-energy balance equation is equivalent to specifying $\partial u_e/\partial x = 0$. Other terms in the energy balance equation such as the energy loss through collisions and joule heating are negligible at the electrodes.

The boundary conditions in time have not been explicitly mentioned. Essentially the simulation is terminated once periodic steady state is attained. Electron kinetics and transport properties are obtained by solving the zero-dimensional Boltzmann equation, with a model for the kinetics of excited states. The electron mobility and diffusion coefficient are actually a function of the electron energy, but do not vary as strongly as the Townsend ionization coefficient. In this work the electron mobility and electron diffusion coefficient are taken to be uniform and time invariant.

III. SOLUTION TECHNIQUE

Direct solution techniques employ either the Gummel-Scharfetter discretization scheme[2] or a Fourier series expansion.[1] The solution technique used here is based on the decoupling of the equations into a set of time-averaged and time-dependent equations.

The overall solution scheme is as follows. Using an initial guess for the spatial profile of the ionization and attachment rates, the time-averaged charged-particle continuity and momentum conservation equations are solved together with Poisson's equation to yield the time-averaged concentrations and fluxes of charged particles, and the electric field within the discharge. Next, the time-dependent electron continuity and momentum conservation equations, and the positive- and negative-ion momentum conservation equations, are solved together with Poisson's equation, for a specified rf discharge current, to yield the time-dependent electron concentration, the charged particle fluxes, the electric field, and the potential within the discharge. This solution also yields the time-dependent power dissipation within the discharge. At this stage the positive- and negative-ion continuity equations do not need to be solved since we are assuming that their concentrations are time invariant and given by their time-averaged value. Finally, the electron-energy balance equation is solved using the calculated power dissipation, and the known time-dependent charged-particle concentrations and fluxes, to yield the time-dependent mean electron energy, and the time-dependent ionization and attachment rates. The time-dependent ionization and attachment rates are time averaged and used to revise the initial estimates for these values. The whole solution procedure is repeated until a self-consistent net ionization rate is obtained. The following sections describe each of these steps in further detail.

A. Time-averaged solution

Time averaging of the equations results in the following set of equations:

$$\frac{d\bar{\Gamma}_e}{dx}=r_i-r_a+k_d n_n N^* \ , \tag{16}$$

$$\frac{d\bar{\Gamma}_p}{dx}=r_i-k_r n_n n_p \ , \tag{17}$$

$$\frac{d\bar{\Gamma}_n}{dx}=r_a-k_r n_n n_p-k_d n_n N^* \ , \tag{18}$$

$$\bar{\Gamma}_e=-\mu_e \bar{n}_e \bar{E}-D_e\frac{d\bar{n}_e}{dx}-\mu_e A(x) \ , \tag{19}$$

$$\bar{\Gamma}_p=n_p\bar{v}_p=\mu_p n_p \bar{E} \ , \tag{20}$$

$$\bar{\Gamma}_n=n_n\bar{v}_n=-\mu_n n_n \bar{E} \ , \tag{21}$$

$$\frac{d\bar{E}}{dx}=\frac{e}{\epsilon_0}(n_p-n_n-\bar{n}_e) \ . \tag{22}$$

In the above equations, variables without the overbar are assumed to be time invariant, except for r_i and r_a, which represent time-averaged quantities. It is important to note that both the positive and negative ions have been treated as time invariant. This assumption fails at frequencies below ~ 1 MHz when the ion concentration is modulated by the time-varying field.[9] Also, the electron and ion transport properties are taken to be uniform and time invariant. Time averaging of the electron continuity equation [Eq. (1)] requires an averaging of the quantity $n_e E$. This term has been split into two terms, such that

$$\overline{n_e E}=\bar{n}_e\bar{E}+A(x) \ , \tag{23}$$

where $A(x)$ is taken to be zero for the first iteration; for subsequent iterations it is evaluated from the time-dependent solution obtained in the preceding iteration.

The corresponding time-averaged boundary conditions are

$$\bar{\Gamma}_e=\mp S\bar{n}_e-\gamma\bar{\Gamma}_p \ , \tag{24}$$

$$\frac{d^2\bar{E}^2}{dx^2}=0 \ , \tag{25}$$

$$\bar{\Gamma}_n=0 \ , \tag{26}$$

$$\bar{\Gamma}_p-\bar{\Gamma}_n-\bar{\Gamma}_e=0 \ . \tag{27}$$

The current constraint emphasizes that the number of positively and negatively charged particles leaving the plasma, when averaged over the cycle, must be equal, so that the plasma remains electrically neutral. The algorithms used for solving these time-averaged equations differ for electropositive and electronegative gases, and are the subject of Secs. III A 1 and II A 2.

1. *Electropositive gases*

In electropositive gases, attachment is zero, and terms representing attachment, detachment, and ion-ion recombination are absent. The set of equations [Eqs. (16)–22)] are solved using an approach first developed for electron beam sustained glow discharges,[15] and modified for parallel-plate rf glow discharges.[8] The main features of the technique are reiterated here.

After appropriate algebraic manipulation[16] the time-averaged equations can be reduced to an ordinary differential equation for the electric field, which is

$$\mu_p\left[\bar{n}_e+\frac{\epsilon_0}{e}\frac{d\bar{E}}{dx}\right]\bar{E}=R(x)-R(d/2) \ , \tag{28}$$

where the expression for $\bar{n}_e$ in terms of the electric field is

$$\bar{n}_e=\frac{(1+\gamma)R(d/2)}{S}-\frac{1}{D_e}\left[\left[1+\frac{\mu_e}{\mu_p}\right]\left[P(x)+\frac{x}{d}P(x)\right]+\mu_e B(x)-\frac{\epsilon_0\mu_e}{2e}[\bar{E}^2(x)-\bar{E}^2(0)]\right] \ . \tag{29}$$

The auxiliary terms $R(x)$, $P(x)$, and $B(x)$ are defined as

$$R(x)=\int_0^x r_i dx \ , \tag{30}$$

$$P(x)=\int_0^x R(x)dx \ , \tag{31}$$

$$B(x)=\int_0^x A(x)dx \ , \tag{32}$$

These terms can be evaluated since initial guesses for the ionization rate r_i and the correction factor $A(x)$ are available. These are known either from a previous iteration or have to be estimated for the first iteration. For the first iteration $A(x)$ is simply set to zero, while r_i is estimated from a previous simulation. An approximate solution, explained in Sec. III D, is used to refine the estimate for r_i to speed up convergence. If one substitutes the expressions for $R(x)$, $P(x)$, and $B(x)$ into Eq. (29) and the resulting expression for $\bar{n}_e$ into Eq. (28), an ordinary differential equation for the electric field results. The boundary condition expressed by Eqs. (24) and (27) have been used in deriving Eq. (29). The remaining boundary condition [Eq. (25)] is used to solve the differential equation for $\bar{E}$. The differential equation, when finite differenced, results in a set of coupled nonlinear algebraic equations for the electric field. This set of equations can be solved very efficiently using the Newton-Raphson technique for a system of nonlinear equations. Terms that appear off the central band in the Jacobian can be neglected. Only elements that lie along the three central diagonals need to be included in the Jacobian.

For any nonlinear system of equations an initial guess is required. This initial guess is generated by setting ϵ_0 to zero in Eq. (29), and solving the resulting expression for $\bar{n}_e$. Setting ϵ_0 to zero is equivalent to assuming quasineutrality ($n_p=\bar{n}_e$):

$$\bar{n}_e=\frac{(1+\gamma)R(d/2)}{S}-\frac{1}{D_e}\left[1+\frac{\mu_e}{\mu_p}\right]\left[P(x)-P(d)\frac{x}{d}\right] , \tag{33}$$

$$\bar{E}(x)=\frac{R(x)-R(d/2)}{\mu_p\bar{n}_e} \ . \tag{34}$$

Thus a guess for $\bar{n}_e$ is obtained from Eq. (33) and the initial estimate for $\bar{E}(x)$ is obtained from Eq. (34). Convergence is usually achieved within 50 iterations, and is speeded up if the value of S is gradually increased from 10^5 cm/s to its final value over about 10 iterations. Once $\bar{E}(x)$ has been determined $\bar{n}_e$ is evaluated using Eq. (29), and the other time-averaged variables are calculated using

$$n_p=\bar{n}_e+\frac{\epsilon_0}{e}\frac{d\bar{E}}{dx} \ , \tag{35}$$

$$\bar{\Gamma}_p=\bar{\Gamma}_e=R(x)-R(d/2) \ . \tag{36}$$

In this fashion, all the time-averaged properties of an electropositive discharge are readily evaluated.

2. *Electronegative gases*

In electronegative gases, attachment, ion-ion recombination, and detachment are important. In the case of electropositive gases an initial estimate for the spatial profile of the ionization rate is required. If the same scheme is extended to electronegative gases, estimates for the spatial profile of the ionization, attachment, ion-ion recombination, and detachment rates are required. Besides being very cumbersome, a fundamental difficulty is encountered. In an electronegative discharge, negative ions cannot overcome the retarding potential of the sheaths, and are trapped within the plasma. Negative ions formed through attachment must be destroyed entirely through ion-ion recombination and detachment. Thus the total attachment within the discharge must be equal to the total ion-ion recombination and detachment. This implies that any arbitrarily specified spatial profile for these quantities must satisfy this constraint. Actually only a unique solution is possible and that is the self-consistent solution. This suggests that at least some of the spatial profiles must be generated as a part of the solution. The others may be specified independently. The algorithm presented here has been developed for gases like SF_6 in which ion-ion recombination dominates detachment. Thus detachment is neglected in the analysis that follows.

Rather than specify the spatial profile of the ionization rate alone, the spatial profile of the attachment rate is specified as well. By generating an estimate for the mean electron energy and the electron number density in the discharge, the spatial profiles of the ionization and attachment rates can be estimated. Fortunately, in electronegative gases, both the mean electron energy and electron number density are very nearly uniform across the discharge, so if results from a previous simulation are unavailable, a uniform profile for the ionization and attachment rates may be assumed. This kind of spatial profile is adequate for a first guess. Naturally the ionization rate must exceed the attachment rate for a solution to exist since some electrons reach the electrodes. An approximate solution, explained in Sec. III D is used to refine the estimates for r_i and r_a to speed up convergence. It is based on a zero-dimensional solution of the continuity and momentum conservation equations, coupled with the electron-energy balance equation. In short, estimates of the spatial profile for the ionization and attachment rates can be generated.

After suitable algebraic manipulation,[16] Eqs. (16)–(22) can be recast as

$$\frac{d(n_n\bar{E})}{dx}+\frac{r_a-k_r n_n(n_n+\bar{\rho}+\bar{n}_e)}{\mu_n}=0 \ , \tag{37}$$

$$\frac{d[(\bar{\rho}+\bar{n}_e)\bar{E}]}{dx}-\frac{r_i-k_r n_n(n_n+\bar{\rho}+\bar{n}_e)}{\mu_p}-\frac{r_a-k_r n_n(n_n+\bar{\rho}+\bar{n}_e)}{\mu_n}=0 \ . \tag{38}$$

Equations (37) and (38) are differential equations for $\bar{n}_e$ and n_n, but also include other variables such as $\bar{E}$ and $\bar{\rho}$. These two variables may be eliminated using the following expressions:

$$\bar{E}=\frac{-D_e(d\bar{n}_e/dx)-\mu_e A(x)}{\mu_p n_p+\mu_n n_n+\mu_e \bar{n}_e} , \tag{39}$$

$$\bar{\rho}=\frac{\epsilon_0}{e}\frac{d\bar{E}}{dx} . \tag{40}$$

Thus, for the case of electronegative gases, the time-averaged equations simplify to a set of coupled, second-order differential equations for the electron and negative-ion concentrations. The appropriate boundary conditions are

$$\mp\int_0^{d/2}(r_i-r_a)dx=\mp S\bar{n}_e , \tag{41}$$

$$\bar{\Gamma}_n=0 . \tag{42}$$

The boundary condition $\bar{\Gamma}_n=0$ is equivalent to $n_n=0$, as explained earlier. When Eqs. (37) and (38) are finite differenced, a set of coupled nonlinear algebraic equations for $\bar{n}_e$ and n_n are obtained, which once again are solved using the Newton-Raphson technique. By organizing the solution vector in terms of the tuples $(\bar{n}_e,n_n)$, and ordering the equations so that the equations for variables at the grid point j immediately precede the equations for variables at $j+1$, a compact Jacobian is obtained. Typically only elements lying along the 10 principal diagonals of the matrix need to be considered. As before, initial guesses for $\bar{n}_e$ and n_n are required.

Initially the attachment rate is set to zero, the ion-ion recombination rate constant is set to a high value ($k_r>10^{-5}$ cm^3/s), ϵ_0 is set to zero, and N_n is also set to zero. Since attachment is zero, the algorithm for an electropositive gas is used to generate the electron and positive-ion concentrations. Once these have been obtained then the finite-differenced form of Eqs. (37) and (38) are solved in stages. First the attachment rate is increased to its full value in approximately eight steps, then the recombination rate constant is raised to its final value in approximately eight steps, and finally ϵ_0 is increased to its actual value over approximately 20 steps. Overall convergence is achieved within approximately 50 steps. However, since we are solving a much larger matrix than for the electropositive discharge, solution times for the time-averaged solution are significantly longer. In electropositive gases the time-averaged solution is obtained relatively quickly compared to the time-dependent solution. In electronegative gases the computational complexity of the time-averaged solution is comparable to the complexity of the time-dependent solution. Overall, the solution for electronegative gases is slower by a factor of 3. Once $\bar{n}_e$ and n_n have been determined, the time-averaged field is evaluated using Eq. (39), and the other time-averaged variables are calculated according to

$$n_p=n_n+\bar{n}_e+\frac{\epsilon_0}{e}\frac{d\bar{E}}{dx} , \tag{43}$$

$$\bar{\Gamma}_p=\int_{d/2}^{x}(r_i-k_r n_n n_p)dx , \tag{44}$$

$$\bar{\Gamma}_n=\int_{d/2}^{x}(r_a-k_r n_n n_p)dx , \tag{45}$$

$$\bar{\Gamma}_e=\bar{\Gamma}_p-\bar{\Gamma}_n . \tag{46}$$

As an aside it is interesting to study the implication of Eq. (39) regarding the electron number density distribution in the sheath of an electropositive discharge. Neglecting $A(x)$, a simplified expression for $E(x)$ is

$$\bar{E}=\frac{-D_e(d\bar{n}_e/dx)}{\mu_p n_p+\mu_e \bar{n}_e} . \tag{47}$$

In the plasma $n_p\approx\bar{n}_e$. Since $\mu_p\ll\mu_e$, expanding Eq. (47) and neglecting $\mu_p n_p$,

$$-\mu_e\bar{n}_e\bar{E}-D_e\frac{d\bar{n}_e}{dx}=0 . \tag{48}$$

This implies that in the plasma, electron drift is balanced by electron diffusion. If Eq. (48) is integrated, the Boltzmann relation for the electron number density distribution ($\bar{n}_e=\bar{n}_{e0}e^{V/T_e}, T_e=D_e/\mu_e$) is obtained. In the sheaths $n_p\gg\bar{n}_e$. Therefore neglecting $\mu_e\bar{n}_e$ instead and expanding Eq. (47) as before, we find that the electron concentration is no longer given by the Boltzmann relationship. Thus if electron and ion motion through the sheath is collision dominated, the electrons *do not* satisfy the Boltzmann relationship. In the plasma they generally obey the Boltzmann relationship.

B. Time-dependent solution

Once the time-averaged variables have been computed, the time-dependent equations are solved to obtain the time-varying variables within the discharge. The continuity equations for the positive and negative ions do not need to be solved since the time-invariant ion concentrations have already been determined from the time-averaged solution. The final forms of the equations are restated here for convenience.

$$\frac{\partial n_e}{\partial t}+\frac{\partial\Gamma_e}{\partial x}=r_i-r_a , \tag{49}$$

$$\Gamma_e=-\mu_e n_e E-D_e\frac{\partial n_e}{\partial x} , \tag{50}$$

$$\frac{1}{\nu_h}\frac{\partial v_p}{\partial t}+v_p=\mu_p E , \tag{51}$$

$$\frac{1}{\nu_h}\frac{\partial v_n}{\partial t}+v_n=-\mu_n E , \tag{52}$$

$$\frac{\partial E}{\partial x}=\frac{e}{\epsilon_0}(n_p-n_n-n_e) . \tag{53}$$

Boundary conditions at the electrodes are

$$\Gamma_e=\mp Sn_e-\gamma\Gamma_p , \tag{54}$$

$$\Gamma_e=\frac{J_{c0}}{e}\cos(\omega t)=\Gamma_p-\Gamma_n-\Gamma_e+\frac{\epsilon_0}{e}\frac{\partial E}{\partial t} . \tag{55}$$

Substituting $\Gamma_p=n_p v_p$, $\Gamma_n=n_n v_n$, and Eq. (50) for Γ_e into Eq. (55), and expressing n_e in terms of n_p and n_n using Eq. (53), one obtains a differential equation for the electric field, which is second order in space and first order in time. The equation and associated boundary conditions are

$$v_p n_p - v_n n_n + \frac{\epsilon_0}{e}\frac{\partial E}{\partial t} - \frac{J_{c0}}{e}\cos(\omega t) = -D_e \frac{\partial}{\partial x}\left[n_p - n_n - \frac{\epsilon_0}{e}\frac{\partial E}{\partial x}\right] - \mu_e\left[n_p - n_n - \frac{\epsilon_0}{e}\frac{\partial E}{\partial x}\right]E , \quad (56)$$

$$\Gamma_e = \mp S n_e - \gamma \Gamma_p . \quad (57)$$

The boundary condition [Eq. (57)] is expressed purely in terms of the electric field by employing the following relations:

$$n_e = n_p - n_n - \frac{\epsilon_0}{e}\frac{\partial E}{\partial x} , \quad (58)$$

$$\Gamma_e = v_p n_p - v_n n_n + \frac{\epsilon_0}{e}\frac{\partial E}{\partial t} - \frac{J_{c0}}{e}\cos(\omega t) . \quad (59)$$

At first glance it might seem as if the electron continuity equation has been neglected; this is not the case since the current constraint [Eq. (55)] is obtained by combining the continuity equations for charged particles. Naturally a periodic steady state is the boundary condition in time. Equation (56) is finite differenced using the unconditionally stable Crank-Nicholson scheme. In order to balance the spatial and temporal errors, so that the finite-difference scheme is accurate to second order, the period is divided into 200 time steps and the electrode spacing into 61 elements. The elements are unequally sized, with the grid size increasing by a constant factor (~ 1.2) from the electrode towards the center of the discharge. For convenience the same grid layout is used to solve the time-dependent electron-energy balance equation and the set of time-averaged equations. The set of nonlinear finite-differenced equations is once again solved using the Newton-Raphson technique. The time variable is advanced until a periodic steady state is attained. At each time step the positive- and negative-ion velocities and fluxes are advanced using

$$v_p(x,t) = v_p(x,t-\Delta t)e^{-\nu_h \Delta t} + \mu_p E(1 - e^{-\nu_h \Delta t}) , \quad (60)$$

$$v_n(x,t) = v_n(x,t-\Delta t)e^{-\nu_h \Delta t} - \mu_n E(1 - e^{-\nu_h \Delta t}) , \quad (61)$$

$$\Gamma_p = n_p v_p , \quad (62)$$

$$\Gamma_n = n_n v_n . \quad (63)$$

The instantaneous electric field is used in Eqs. (60) and (61). Examination of Eqs. (60) and (61) shows that if $e^{-\nu_h \Delta t} \sim 1$, the ions do not respond to the instantaneous electric field. In the opposite limit, if $e^{-\nu_h \Delta t} \ll 1$, ions respond to the instantaneous field. At rf frequencies exceeding ~ 10 MHz the former situation prevails.

Once a periodic steady state is achieved, the sequence of values of E, v_p, and v_n over the period of the cycle constitute the solution. Then n_e is evaluated using Eq. (58) and Γ_e is calculated using Eq. (59). Finally, assuming that the grounded electrode is at $x = 0$, the discharge potential V is calculated according to

$$V(x) = -\int_0^x E\, dx . \quad (64)$$

In order to apply the Crank-Nicholson technique, an initial condition is required for E. Also, the initial ion velocities need to be specified in order to advance the solution using Eqs. (60) and (61). Since in many discharges, the discharge impedance is more capacitive than resistive, the phase angle between the voltage and current waveforms is closer to $-90°$ and to $0°$. By choosing the form of the driving current as $J_{c0}\cos(\omega t)$ rather than $J_{c0}\sin(\omega t)$, a good guess for $E(x,0)$ is $E(x,0) = \bar{E}(x)$. Specifying the time-averaged variables of the discharge as the initial conditions, implies that $E = \bar{E} + E_0 \sin(\omega t)$. Since $J_c \approx \epsilon_0 \partial E/\partial t$ in the sheaths (and the total discharge current is continuous), this implies that $J_c = J_{c0}\cos\omega t$. Then the initial positive- and negative-ion velocities are $v_p = \mu_p \bar{E}(x)$ and $v_n = -\mu_n \bar{E}(x)$. With these initial conditions, a periodic steady state is achieved within five rf cycles.

Once the discharge properties have been obtained for the assumed spatial profile, all that remains is an evaluation of the self-consistent ionization and attachment rates. This is done by solving the time-dependent electron-energy balance equation. This equation and appropriate boundary condition are

$$\frac{\partial(n_e u_e)}{\partial t} + \frac{5}{3}\frac{\partial(\Gamma_e u_e)}{\partial x} - \frac{2}{3}\frac{\partial(K_e/k)}{\partial x}\frac{\partial u_e}{\partial x} + \Gamma_e E + k_\epsilon(u_e) n_e N = 0 , \quad (65)$$

$$\frac{\partial u_e}{\partial x} = 0 . \quad (66)$$

This boundary condition is equivalent to Eq. (15), as discussed earlier.

In the energy balance equation, all quantities except u_e are known at this stage. This equation, when finite differenced according to the Crank-Nicholson scheme, results in a system of nonlinear equations for u_e. The system is solved by the Newton-Raphson method as before. The time variable is advanced until a periodic steady state is reached. Convergence to steady state is usually achieved within four cycles. Over most of the discharge, the joule heating ($-\Gamma_e E$) balances the electron loss through elastic and inelastic collisions [$k_\epsilon(u_e) n_e N$]. The initial guess for the electron energy is obtained by equating the power deposition (if positive) to the electron-energy-loss rate,

$$k_\epsilon(u_e)\bar{n}_e N + \overline{\Gamma_e E} = 0 . \quad (67)$$

In regions where the joule heating is negative (electrons are diffusing against the field), the initial guess for the mean electron energy is set equal to the gas temperature in eV. Finally, the self-consistent spatial profiles of the time-averaged ionization and attachment rates are calculated according to

$$r_i = \frac{1}{T}\int_0^T k_i n_e N\, dt , \quad (68)$$

$$r_a = \frac{1}{T}\int_0^T k_a n_e N\, dt . \quad (69)$$

The previous estimates for the ionization and attachment rates are revised on the basis of these newly calculated spatial profiles, and the entire solution (time averaged and time dependent) is repeated until satisfactory convergence is achieved. When changes in the total net ionization between successive iterations is less than 10%, convergence is assumed. With a good initial guess, convergence is achieved in less than five loops through the entire sequence of solutions.

C. Convergence

The use of the Newton-Raphson and Crank-Nicholson techniques assures convergence for the time-averaged and time-dependent solutions, provided the initial guesses are within the domain of convergence. However, the convergence of the spatial profiles of the ionization and attachment rates is problematical. No mathematical proof demonstrating convergence of the outer loop has been developed. Rather we shall rely on physical arguments to show that the system tends to converge. If the initial guess for the net ionization rate is too low, the calculated electron number density will also be low. This, in turn, implies a high discharge resistivity (R), and if the discharge current (I) remains unchanged from iteration to iteration, the joule heating (I^2R) will increase. Consequently the predicted ionization rate will be higher than initially assumed. Just like the Newton-Raphson method, the present technique is subject to overshoot. If the solution overshoots, the overshoots can grow and eventually the system becomes divergent. Therefore it is vital to start with a good initial guess and to limit the overshoot. The second method with underrelaxation is used to generate the new estimates for the ionization and attachment rates, given the values for the previous two iterations. This technique exhibits desirable convergence characteristics.

One problem plaguing solutions in electronegative gases is that if the mean electron energy is too low, the time-averaged attachment rate exceeds the time-averaged ionization rate, in the central region of the discharge. This is a nonphysical situation and numerically is manifested as nonphysical solutions. A simple way to fix this problem is to set the ionization rate at least equal to the attachment rate in all regions where there is a surfeit of ionization, and continue the solution. The self-correcting tendency discussed in the preceding paragraph results in a more realistic ionization rate at the end of the iteration.

D. Simplified models

Each outer loop iteration is fairly time intensive. At the end of each outer loop, estimates for the ionization and attachment rates are refined, and the solution is continued. Thus any strategy that either shortens each loop iteration, or helps generate a good initial guess for the ionization and attachment rates, improves computational efficiency. Two schemes are discussed here; the first is specific to discharges in electropositive gases and the second to discharges in electronegative gases.

1. Electropositive gases

The time-dependent solution of the fluid equations is quite time consuming. Thus, rather than solve this set of equations during each iteration, it is prudent to substitute an approximate solution for this module. In this way, once the estimate for the spatial profile of the ionization rate is refined sufficiently, the comprehensive module replaces the simplified module. Usually it takes a couple of outer loop iterations to achieve convergence beyond this point. The simplified module estimates the time-averaged joule heating $-\Gamma_e E$ without solving the time-dependent electron continuity and momentum conservation equations. Once the time-averaged joule heating is known, the time-averaged electron energy balance can be solved to yield the time-averaged mean electron energy and the time-averaged ionization rates. Briefly the scheme is as follows.

Electron conduction current is the dominant mode of current transport in the central region of the discharge, which has an abundant supply of mobile electrons. In other words, the conduction current is equal to the total discharge current. Thus the time-averaged joule heating of the plasma is given by

$$\overline{-\Gamma_e E}=\overline{\left[\frac{J_{c0}^2}{2e\sigma_e}\right]}\ , \tag{70}$$

where σ_e, the electron conductivity, is given by

$$\sigma_e=e\mu_e n_e\ . \tag{71}$$

Over the central region of the discharge, n_e is almost time invariant and is thus given by its time-averaged value $\bar{n}_e$. Then the time-averaged joule heating can be expressed solely in terms of quantities evaluated from the time-averaged solution. The final expression for the joule heating is

$$-\overline{\Gamma_e E}=\frac{J_{c0}^2}{2e^2\mu_e\bar{n}_e}\ . \tag{72}$$

This expression fails in the sheaths; in fact, the expression predicts infinite joule heating at the electrode for $\bar{n}_e\to 0$. The expression is invalid because displacement current dominates current transport in the sheath. At the electrode, joule heating is negative (electrons are cooling off as they diffuse against the field) and is $\sim -\bar{\Gamma}_e\bar{E}$. Equation (72) is assumed to hold in all regions, except the sheaths. The sheath edge is defined as the point where the ratio of the electron number density to the ion number density is 0.95. This definition is quite arbitrary, but appears to give good results. Since the electron number density decays rapidly towards the electrodes, the exact number is not very critical. In all other regions a linear interpolation between the joule heating at the electrode and its value at the sheath edge calculated from Eq. (72) is used. A linear fit is suggested by the full solution.

Given the joule heating, the time-averaged electron-energy balance equation yields the time-averaged mean electron energy,

$$\frac{5}{3}\frac{d(\overline{\Gamma}_e\overline{u}_e)}{dx}-\frac{2}{3}\frac{d(\overline{K}_e/k)}{dx}\frac{d\overline{u}_e}{dx}+\overline{\Gamma_e E}+k_\epsilon(\overline{u}_e)\overline{n}_e N=0 . \tag{73}$$

The associated boundary condition is

$$\frac{d\overline{u}_e}{dx}=0 . \tag{74}$$

The time-averaged electron-energy balance equation is finite differenced, and the resulting set of nonlinear equations were solved using the Newton-Raphson technique. Convergence is achieved within a few iterations. The initial guess for the mean electron energy is obtained by equating the power deposition (if positive) to the electron-energy-loss rate

$$k_\epsilon(\overline{u}_e)\overline{n}_e N+\overline{\Gamma_e E}=0 . \tag{75}$$

In regions where the joule heating is negative (electrons are diffusing against the field), the initial guess for the mean electron energy is set equal to the gas temperature in eV, as before. Finally the time-averaged ionization rate is calculated according to

$$r_i=k_i(\overline{u}_e)\overline{n}_e N . \tag{76}$$

2. Electronegative gases

In electronegative gases, the time-averaged solution is also time consuming. Also, if the estimates for the ionization and attachment rates are poor, nonphysical results are generated. Thus realistic estimates for the ionization and attachment rates are essential. Unlike in the case of electropositive gases, the time-dependent equations must be solved. At any instant during the rf cycle, the ionization and attachment rates differ, but when averaged over the cycle, they are almost equal. When the electric field is high, ionization dominates attachment, while attachment dominates during that portion of the cycle when the electric field is low. Fortunately, since electron loss through diffusion is small compared to loss through attachment, the electron number density is fairly uniform across the discharge. Thus to first order, the spatial gradient terms can be neglected. A scheme based on these concepts has been developed for SF_6 discharges.[17] The approach presented here is a modified version of the original formulation.

As in the case of electropositive gases, electron conduction current dominates displacement current, and ion current, in the central region of the discharge. Under these conditions the electron continuity and momentum conservation equations become

$$\frac{dn_e}{dt}=[k_i(u_e)-k_a(u_e)]n_e N , \tag{77}$$

$$J_{c0}\cos(\omega t)=-e\mu_e n_e E . \tag{78}$$

Integrating Eq. (77) and substituting for n_e in Eq. (78) we get

$$E(t+\Delta t)=\frac{\cos[\omega(t+\Delta t)]}{\cos\omega t}E(t)e^{-[k_i(u_e)-k_a(u_e)]N\Delta t} . \tag{79}$$

Starting with the initial condition $E(0)=(E/N)_c N$, $(E/N)_c$ is the reduced electric field for which the Townsend ionization and attachment coefficients are equal, and it is equal to $\sim 375\times 10^{-17}$ V cm^2 for SF_6. A mean electron energy u_e, corresponding to $(E/N)_c$, the electric field, is advanced using Eq. (79), and at each time step, u_e is also advanced through an implicit Euler solution of

$$\frac{du_e}{dt}-\mu_e E^2+k_\epsilon(u_e)N=0 . \tag{80}$$

Equation (80) is a modified form of the electron-energy balance equation [Eq. (8)], with the spatial derivatives dropped. The solution is advanced over several cycles until periodic steady state is attained. Finally, the electron number density and the time-averaged ionization and attachment rates are calculated using

$$n_e=-\frac{J_{c0}\cos(\omega t)}{e\mu_e E(t)} , \tag{81}$$

$$r_i=\frac{1}{T}\int_0^T k_i(u_e)n_e N\,dt . \tag{82}$$

$$r_a=\frac{1}{T}\int_0^T k_a(u_e)n_e N\,dt . \tag{83}$$

3. Solution time

The simplified solution schemes presented above are very efficient computationally. In electropositive discharges, the time-averaged solution of the continuity and momentum conservation equations, together with the simplified formulation of the time-dependent equations, takes less than a minute to compute on a Micro Vax II. Similarly, the zero-dimensional solution of the time-dependent continuity and momentum conservation equations for an electronegative gas also require less than a minute to compute. Thus every solution of the full set of equations is preceded by a solution of the simplified forms of the equations.

IV. KINETICS AND TRANSPORT DATA

A number of kinetics and transport properties, such as mobilities, diffusion coefficients, rate constants for ionization, attachment, detachment, recombination, and electron energy loss, have to be known before the transport equations can be resolved. These properties are specific to the gas, and can be computed or obtained from the literature. In this work, simulations have been performed in Ar and SF_6 discharges.

Electron-impact ionization of excited atomic or molecular states can constitute a significant fraction of the total ionization, especially if any of the excited states are metastable states. In argon, ionization from the metastable levels dominated over direct ionization from the ground state at low values of E/N. The threshold for ionization from metastable levels (4.2 eV) is much lower than the

threshold for ionization from the ground state (15.8 eV). Thus excited-state populations enhance the Townsend ionization coefficient through additional ionization arising from these states. Also superelastic collisions of the electrons with these excited states populate the tail of the distribution function, thereby increasing the amount of direct ionization. Experimentally, Townsend coefficients are measured in drift tube and swarm experiments, in which the population of excited states is negligible. Thus such experimental data for the Townsend ionization coefficient may be lower than the effective value for the ionization coefficient in the discharge.

More realistic values for the Townsend ionization coefficient may be obtained by solving a kinetics model for the excited states in conjunction with the Boltzmann equation for each value of E/N. Generally, most excited states, except for metastable states, constitute too small a mole fraction to affect the total ionization coefficient. Thus it is sufficient to solve rate equations only for the metastable states, to determine self-consistent values for the metastable mole fractions for each value of E/N. The total Townsend ionization coefficient corresponding to these metastable mole fractions is the effective Townsend ionization coefficient. Electron kinetics and transport data in argon are obtained by solving the Boltzmann equation in conjunction with a four-level collisional-radiative model.[16]

In molecular discharges the actual gas composition can be quite different from the composition of the feed gases as a result of electron-impact dissociation and subsequent gas phase and surface reactions. Electron-impact processes and subsequent gas phase chemistry in SF_6 discharges generate a wealth of neutral and excited species. Kinetics models[18,19] predict that over 80% of the SF_6 is dissociated into SF_x fragments, while experimental evidence suggests that less than 30% of the SF_6 is dissociated at pressures exceeding 600 mTorr.[20] In the face of uncertainty regarding the gas phase and electron kinetics it is not feasible to formulate a detailed kinetics model for the SF_6 discharge. Thus swarm parameters have been calculated neglecting excited states and the products of gas phase chemistry.[16]

V. RESULTS

The intent of this section is to demonstrate that the numerical algorithms presented here give reasonable results. The properties of rf discharges in electropositive and electronegative gases have been discussed extensively in other papers.[2,5,9] The results presented in this section have been obtained for parallel-plate symmetric 13.56-MHz rf discharges in Ar and SF_6.

The distribution of charged particles (Fig. 1) in the two types of discharges differs considerably. In electropositive gases electron-impact ionization is balanced by ambipolar diffusion to the electrodes. Thus the charged-particle concentrations exhibit gradients across the discharge. In contrast, in electronegative gases, electron-impact ionization is balanced by electron attachment, and the charged-particle concentrations are essentially uniform across most of the discharge. In electronegative gases the positive- and negative-ion concentrations can exceed the electron concentration by up to two orders of magnitude. The electron concentration is almost time invariant over most of the discharge, and is modulated strongly only in the sheaths. Electronegative gases also exhibit thinner sheaths compared to electropositive gases, in accordance with experimental observations. The electron number densities for $t=0.5$ and 1.0 are the same at each location as can be expected from the symmetry of the applied current waveform (the discharge current is zero at these instants). In all the plots, the time is referenced to the current waveform, which is of the form $J_{c0}\cos(\omega t)/T$. In electropositive gases the electron and positive-ion concentrations peak at the center of the discharge, once again exemplifying that electron loss occurs through ambipolar diffusion. In an electronegative gas, positive ions are lost primarily through ion-ion recombination. Since the ionization rate peaks near the plasma-sheath boundaries and $k_r n_n n_p \approx r_i$, the ion concentrations also peak at the same location.

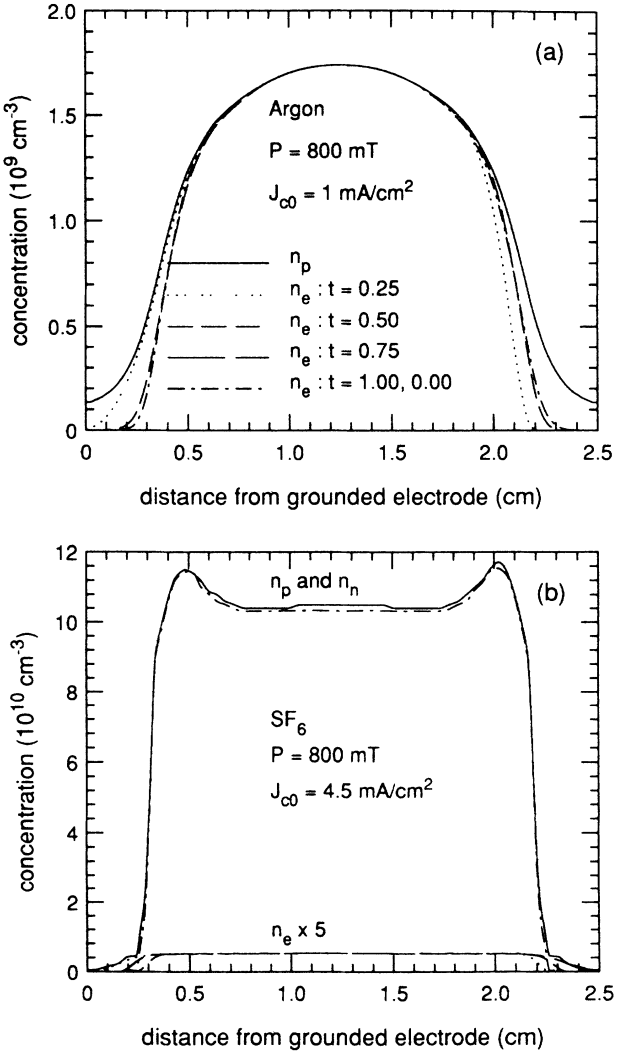

FIG. 1. Charged-particle concentrations in (a) an argon discharge and (b) an SF_6 discharge.

In both types of discharges electron conduction current is the dominant mode of current transport in the plasma. Electrons rather than ions constitute the primary charge carriers due to their higher mobility. Even in electronegative discharges, in which the ion concentration far exceeds the electron number density, electron conduction current is still dominant. This is because the ions respond only to the time-averaged field, while the electrons respond to the instantaneous field. At the center of the discharge, the time-averaged field is zero, while the instantaneous field is nonzero, except at $t=0.25$ and 0.75. In general, the time-averaged field is much smaller than the instantaneous field, except in the sheaths. At the electrode surface the time-averaged field is approximately half the peak value of the time-varying field. There, the displacement current dominates the ion current. Displacement current dominates in the sheath due to the low electron concentration and the low positive-ion mobility. The spatial distribution of the electron conduction current density is shown in Fig. 2. The spatial distributions in Ar and SF_6 discharges are qualitatively similar.

The power dissipation and hence the ionization rate peak near the plasma-sheath interface. In electropositive gases the peak is accentuated compared to the more uniform profile of the ionization rate in electronegative gases (Fig. 3). As expected, electron attachment balances ionization, and ion-ion recombination balances attachment in an electronegative discharge. None of the negative ions have sufficient energy to cross the potential barrier presented by the sheath; thus every negative ion formed through attachment must be consumed by recombination. Since ionization exceeds ion-ion recombination, the time-averaged positive-ion flux is directed towards the electrodes. In contrast, the negative-ion flux is directed towards the center of the discharge, since ion-ion recombination exceeds attachment. Of course, ionization must exceed attachment, and thus the time-averaged electron

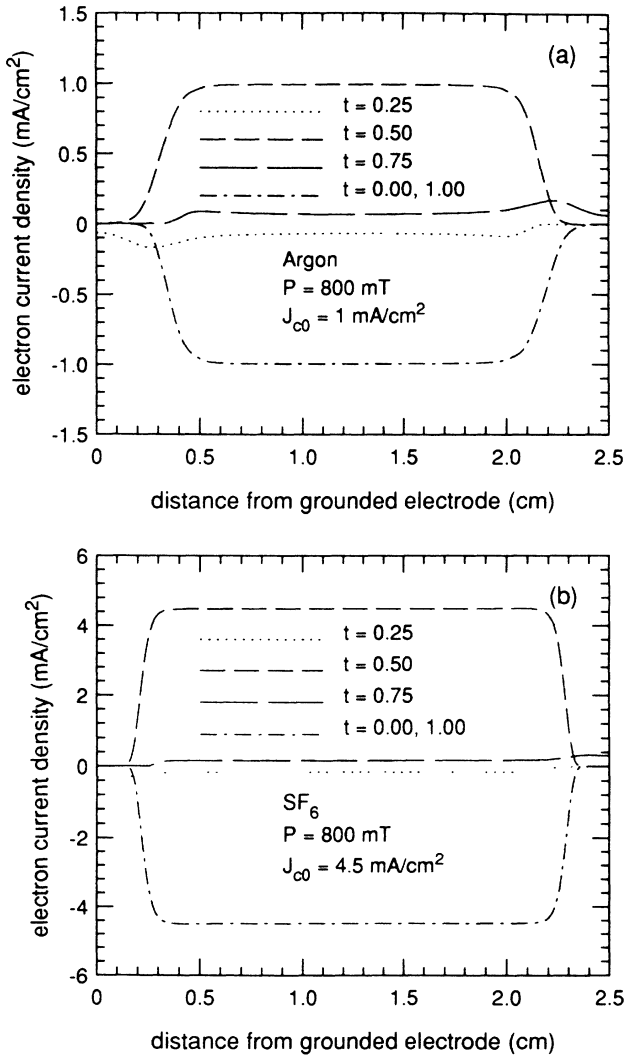

FIG. 2. Electron conduction current density in (a) an argon discharge and (b) an SF_6 discharge.

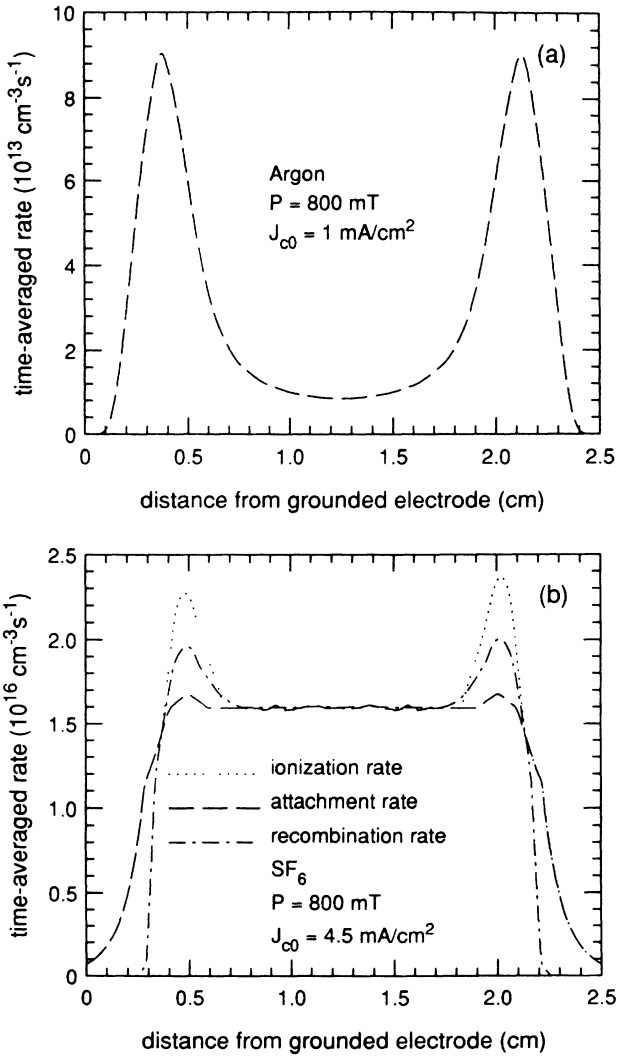

FIG. 3. (a) Time-averaged ionization rate in an argon discharge and (b) time-averaged ionization, attachment, and recombination rates in an SF_6 discharge.

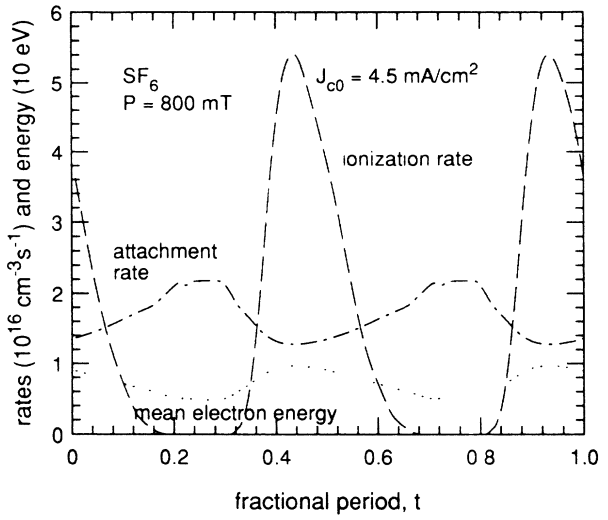

FIG. 4. Ionization and attachment rates at the center of an SF_6 discharge.

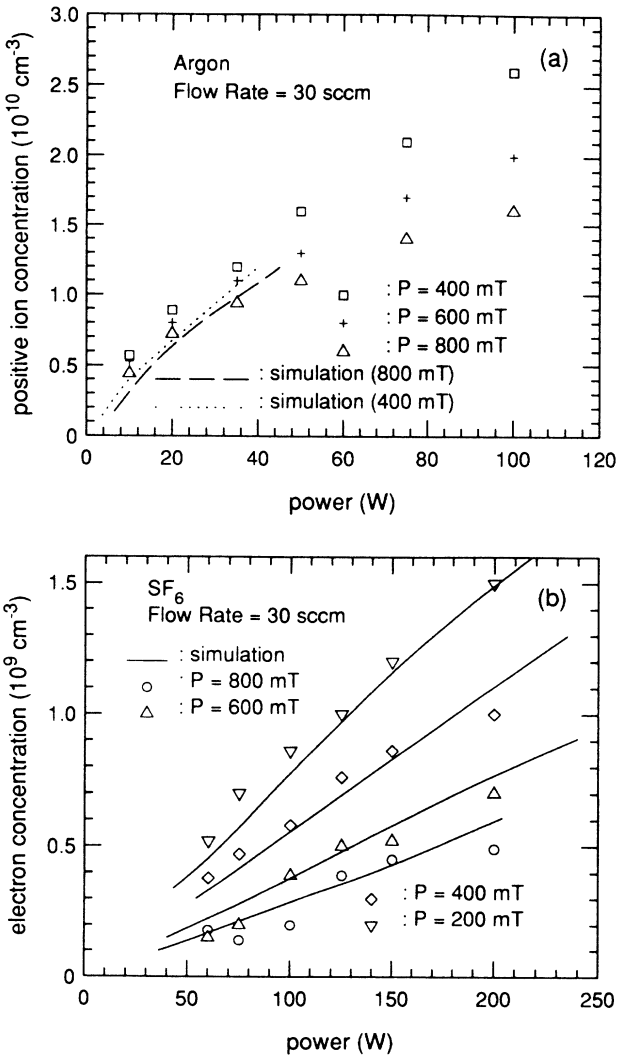

FIG. 5. Calculated and measured electron concentrations (a) an argon discharge and (b) an SF_6 discharge.

flux is directed towards the electrodes. Plasma luminosity, which originates from excited states formed through electron-impact excitation, should correlate with the ionization profile across the discharge. Spatially resolved optical emission from rf discharges in electropositive and electronegative gases support this observation.[5] In the center of the discharge, the mean electron energy is modulated by less than 0.5 eV for argon, but varies between 5 and 10 eV for SF_6, over the period of the cycle. This modulation is reflected in the tremendous variation of the ionization and attachment rates in the center of the discharge (Fig. 4). The modulation in electron energy is such that the net ionization rate averaged over the cycle is almost zero. As expected, optical emission at the center of an SF_6 discharge is modulated strongly, while optical emission at the center of an argon discharge is hardly modulated.[5] Thus, in electropositive discharges, the mean electron energy is modulated only slightly at the discharge center, but can be modulated strongly near the sheaths. In contrast, the mean electronegative discharges is modulated at all locations within the discharge.

Additional properties of rf discharges are reported elsewhere.[16] All the characteristic features discussed here are in agreement with those reported by other workers.[5,9] In addition, Langmuir probe measurements, using a recently developed technique that minimizes rf induced distortion of the probe characteristic have been used to check these calculations.[21] The measured and calculated electron concentrations in Ar and SF_6 discharges are plotted in Fig. 5. The simulation provides the electron number density as a function of the power density (W/cm^2) at the electrode. In order to calculate the electron number density as a function of discharge power, the power density must be multiplied by the electrode area. In an actual discharge, part of the measured power is dissipated in the matching network, and in parasitic discharges. Frequently the discharge is not well confined between the electrodes but balloons towards the chamber walls. Thus the effective discharge area is larger than the actual area of the electrode. Because of these uncertainties, it would be fortuitous for the calculated and measured electron concentrations to agree exactly. Thus, instead of multiplying the calculated power density by the physical electrode area, it has been multiplied by an effective area so as to improve the agreement between the calculated and measured values. In argon the effective discharge area was equal to the physical area of the electrode, while in SF_6 discharges the effective area was 1.5 times as large as the physical area. This does not imply that the Ar discharge is better confined than the SF_6 discharge; in fact, visual observation indicates that quite the opposite is true. Underestimating metastable ionization in argon results in an overprediction of the discharge power. This is the most likely source of error. In any case, the scaling factors, unity for Ar and 1.5 for SF_6, imply that the calculated and measured values agree to within a factor of 2. The calculations predict the trends in electron number density with increasing power quite well. Since the power dissipation is given by $en_e\mu_e E^2$, and both $\mu_e N$ and E/N are independent of pressure, the

slope of the electron concentration versus discharge power increases with decreasing pressure. Numerical instability limited the maximum discharge power in the simulation of argon discharges to 50 W. The exact explanation for the instability is not known. It appears that the correction term $A(x)$, which is introduced in the time-averaged solution becomes comparable to the other terms in the equation as the discharge current (or equivalently power) is increased.

VI. SUMMARY

A fast and numerically stable technique has been developed to simulate 13.56-MHz parallel-plate rf glow discharges in electropositive and electronegative gases. Although results have been shown only for symmetric discharges, the scheme is readily extended to asymmetric discharges. The only significant difference between the symmetric and asymmetric discharges is the dc bias induced on the smaller electrode. Simplified models suitable for generating estimates of the discharge properties have also been developed. These estimates are also used as initial guesses for the full solution. The simplified models execute an order of magnitude faster than the full simulation, but still provide reasonable accuracy. Realistic rate constants for electron-impact processes are obtained by solving the Boltzmann equation in conjunction with models for the kinetics of excited states. Calculated discharge properties, such as the sheath thickness, and the ionization and excitation profiles are in qualitative agreement with experimental findings. Calculated and measured electron number densities agree to within a factor of 2. Calculated and measured electron-energy distribution functions are also in good agreement. Such computationally efficient models are suitable for conducting parametric studies of gas discharges over a range of conditions. These parametric studies have been used to extract scaling laws, which are the subject of a separate paper.[22]

ACKNOWLEDGMENTS

This work was supported by the Semiconductor Research Corporation Contract No. SRC 88-MC-106 and the Defense Advanced Research Projects Agency Contract No. N00014-87-K-0729.

[1]D. B. Graves and K. F. Jensen, IEEE Trans. Plasma Sci. **PB-14**, 78 (1986).
[2]J. P. Boeuf, Phys. Rev. A **36**, 2782 (1987).
[3]A. D. Richards, B. E. Thompson, and H. H. Sawin, Appl. Phys. Lett. **50**, 492 (1987).
[4]M. S. Barnes, T. J. Colter, and M. E. Elta, J. Appl. Phys. **61**, 81 (1987).
[5]E. Gogolides, J. P. Nicolai, and H. H. Sawin, J. Vac. Sci. Technol. A **7**, 1001 (1989).
[6]K. Okazaki, T. Makabe, and Y. Yamaguchi, Appl. Phys. Lett. **54**, 1742 (1989).
[7]D. B. Graves, J. Appl. Phys. **62**, 88 (1987).
[8]A. P. Paranjpe, J. P. McVittie, and S. A. Self (unpublished).
[9]J. P. Boeuf and P. Belenguer, in *Non Equilibrium Processes in Partially Ionized Gases, NATO Advanced Study Institute, Series B: Physics,* edited by M. Capitelli and J. M. Bardsley (Plenum, New York, 1989).
[10]M. S. Barnes, T. J. Cotler, and M. E. Elta, J. Comput. Phys. **77**, 53 (1988).
[11]P. D. Edgley and A. von Engel, Proc. R. Soc. London Ser. A **370**, 375 (1980).
[12]T. Makabe and N. Goto, J. Phys. D **21**, 887 (1988).
[13]C. G. Goedde, A. J. Lichtenberg, and M. A. Lieberman, J. Appl. Phys. **64**, 4375 (1988).
[14]P. M. Chung, Phys. Fluids **12**, 1623 (1969).
[15]A. P. Paranjpe and S. A. Self (unpublished).
[16]A. P. Paranjpe, Ph.D. thesis, Stanford University, 1989 (unpublished).
[17]A. P. Paranjpe, G. Kychakoff, and S. A. Self (unpublished).
[18]L. E. Kline, IEEE Trans. Plasma Sci. **PS-14**, 145 (1986).
[19]H. M. Anderson, J. A. Merson, and R. W. Light, IEEE Trans. Plasma Sci. **PD-14**, 156 (1986).
[20]P. J. Hargis and K. E. Greenberg, Appl. Phys. Lett. **53**, 1809 (1988).
[21]A. P. Paranjpe, J. P. McVittie, and S. A. Self (unpublished).
[22]A. P. Paranjpe, J. P. McVittie, and S. A. Self (unpublished).